

Machine and Process System Diagnostics Using One-Step Prediction Maps

Final Report

Account 3210-002W

Prepared by

B. Damiano
J. E. Breeding
R. W. Tucker, Jr.

June 1999

OAK RIDGE NATIONAL LABORATORY

Post Office Box 2008

Oak Ridge, Tennessee 37831-6007

Research sponsored by the Laboratory Directed Research and Development Program of the Oak Ridge National Laboratory, managed by Lockheed Martin Energy Research Corp. for the U. S. Department of Energy under contract No. DE-AC05-96OR22424

Table of Contents

ABSTRACT	3
1. - INTRODUCTION	3
2. - TECHNICAL BACKGROUND	4
2.1 - Application of Nonlinear Time Series Analysis Techniques	4
2.1.1 - Attractor reconstruction	5
2.1.2 - Mutual information	5
2.1.3 - Method of global false nearest neighbors	6
2.1.4 - Description of radial basis function maps	7
3. - EXAMPLES OF MAP PERFORMANCE	8
3.1 - Example 1 - The Lorenz System	8
3.2 - Example 2 - A Recorded Time Series	10
4. - APPLYING ONE-STEP PREDICTION MAPS TO THE PROBLEM OF MACHINE OR PROCESS SYSTEM DIAGNOSTICS	11
5. - APPLICATION RESULTS	12
5.1 - Test of the Diagnostic Method by Using a Simulated Time Series	12
5.1.1 - Effect of parameter change on the average map error	12
5.1.2 - Effect of adding a sine wave to the time series	13
5.2 - Test of the Diagnostic Method by Using a Measured Time Series	15
5.2.1 - Average absolute map error	15
5.2.2 - Analysis of the Map Error Time Series	16
5.2.2.1 - Analysis of map error power	19
5.2.2.2 - Power ratio - an arcing discriminator	22
6. - SUMMARY	24
6.1 - Research Accomplishments	24
6.2 - Areas for Future Research	25
6.3 - Efforts to Secure Follow-on Funding	26
REFERENCES	27
APPENDIX A	28

LIST OF FIGURES

Figure 1. Comparison of calculated and map-predicted values for the Lorenz system. The values have been normalized to be between +1 and - 1.	9
Figure 2. The normalized time series obtained from the recording.	10
Figure 3. Comparison of the measured and predicted time series for the recorded data.	11
Figure 4. The prediction error for the Lorenz time series. Note the discontinuity at $t = 100$ seconds.	13
Figure 5. Comparison of the map error spectra with and without the added sine wave.	14
Figure 6. Comparison of the spectra of the Lorenz attractor X component with and without the added sine wave.	14
Figure 7. Average absolute map error for different motor current values.	16
Figure 8. FFT magnitude of normalized RF data collected during non-arcing conditions.	18
Figure 9. FFT magnitude for normalized RF data collected during heavy arcing.	18
Figure 10. Variation of map error power in the frequency domain.	19
Figure 11. The map error time series for the baseline time series (file A3.055.txt).	20
Figure 12. Variation of map error power in the time domain. The map error was calculated by using a map formed from the first 50000 points in the baseline time series.	20
Figure 13. Variation of map error power in the time domain. The map error was calculated by using a map formed by using 50000 points beginning at $t = 0.1$ seconds in the baseline time series.	21
Figure 14. FFT magnitude of a map error time series collected during non-arcing conditions.	22
Figure 15. FFT magnitude of a map error time series collected during heavy arcing.	23
Figure 16. Power ratio for conditions ranging from non-arcing to heavy arcing.	23

LIST OF TABLES

Table 1 - Summary of RF Data Files	15
Table 2. Summary of High-Frequency Data Files	17
Table 3. Power Ratio for a Range of Arcing Conditions.	24

Machine and Process System Diagnostics Using One-Step Prediction Maps

ABSTRACT

This report describes a project that investigated a method for machine or process system diagnostics that uses one-step prediction maps. The method uses nonlinear time series analysis techniques to form a one-step prediction map that estimates the next time series data point when given a sequence of previously measured data points. The difference between the predicted and measured values is a measure of the map error. The average value of this error remains within some bound as long as both the dynamic system and its operating condition remain unchanged. However, changes in the dynamic system or operating condition will cause an increase in average map error. Thus, for constant operating conditions, monitoring the average map error over time should indicate when a change has occurred in the dynamic system. Furthermore, the map error itself forms a time series that can be analyzed to detect changes in system dynamics.

The report provides technical background in the nonlinear analysis techniques used in the diagnostic method, describes the creation of one-step prediction maps and their application to machine or process system diagnostics, and then presents results obtained from applying the diagnostic method to simulated and measured data.

1. - INTRODUCTION

This report describes a preliminary investigation of a method for machine or process system diagnostics that uses one-step prediction maps. The main advantages of this method over current predictive maintenance methods are that this method uses time domain data, does not rely on extracting multiple descriptors from the data, and little user expertise is required to interpret the analysis results. We believe these advantages make this method an attractive alternative to current predictive maintenance methods.

Existing diagnostic methods are effective in identifying precursors of equipment failure well in advance of catastrophic failure.^{1,2,3} However, these methods require specialized equipment and highly trained specialists to properly collect and analyze data and to interpret the analysis results. The relatively high overhead costs associated with this type of predictive maintenance, combined with the lack of an accepted method to estimate the resulting cost savings and the management perception that such maintenance programs are not “essential”, has resulted in many predictive maintenance programs being severely cut back or eliminated.^{4,5}

A simpler, less costly, predictive maintenance approach may be an attractive alternative for many applications. The new diagnostic method has the potential for relatively inexpensive implementation requiring a minimum of sensors, specialized equipment, and user expertise. For this reason, we believe the new method may be especially appealing to manufacturing and process

industries that recognize the need and benefits of predictive maintenance programs but are unable to commit the resources required to implement current predictive maintenance practices.

The Technical Background section presents a summary of the nonlinear time series analysis techniques used in the creation of one-step prediction maps along with a description of how one-step prediction maps are formed. This section is followed by a description of how one-step prediction maps are used as a diagnostic tool, forming the basis for the diagnostic method. The Application Results section describes the application of one-step prediction maps as diagnostic tools to simulated and measured time series. The Summary presents conclusions based on the application results.

2. - TECHNICAL BACKGROUND

The diagnostic method uses nonlinear time series analysis techniques to form a map that, given a sequence of time series data points, predicts the next time series point. The map effectively models the dynamics of the system that is generating the time series. Comparison of the predicted values and the subsequently measured values indicates how well the map models these dynamics (assuming noise is negligible). The average difference between the predicted and measured time series values is a measure of the map's error. This error remains within some bound as long as the dynamic system and its forcing function remain unchanged. However, changes in the dynamic system or its forcing function will cause a significant increase in the map error. Thus, monitoring the map error over time should indicate when a change has occurred in either the dynamic system or its forcing functions.

Neither advance knowledge of the system dynamics to detect the system change nor complicated analysis to interpret the results is required. The level of error simply indicates that some system change has occurred between when the one-step prediction map was created and the current measurement. An extension of the technique would involve calculating maps for multiple machine fault conditions and comparing their prediction errors; the condition corresponding to the smallest map error would be identified as being closest to the current machine condition. A brief description of the nonlinear analysis techniques used to create the maps, the map creation itself, and some relevant results from previous work are given in the remainder of this section.

2.1 - Application of Nonlinear Time Series Analysis Techniques

Nonlinear time series analysis techniques are used to determine the optimum time delay used to reconstruct the attractor, and to determine the minimum embedding dimension for reconstruction. If the measured time series is entirely random, any attempt to create a map to approximate and predict the measured time series will be futile. For deterministic systems, the underlying dynamics can be characterized from a time series by applying the method of delays.⁶ The dynamics will usually be multidimensional, with the dimension being initially unknown. Once the

multidimensional attractor is reconstructed from the measured time series, a map that approximates this attractor can be created.

2.1.1 - Attractor reconstruction

Multidimensional attractor reconstruction is performed by using the method of delays.⁶ In this method, vector components are created from a scalar time series by using time series values separated by a delay time. The number of dimensions used in the attractor reconstruction, d_e , is calculated by using global false nearest neighbors and the optimum time delay, τ , equals the time corresponding to the first minimum in the mutual information function. Thus, the i th point of the reconstructed attractor, A_i , is given by

$$A_i = [t(i), t(i - n_{opt}), t(i - 2n_{opt}), \dots, t(i - d_e n_{opt})] \quad (1)$$

where $t(I)$ is the i th time series point and n_{opt} is the number of samples corresponding to τ .

2.1.2 - Mutual information

It is generally accepted that the optimum time delay, τ , used to reconstruct an attractor from a time series corresponds to the time at which the first minimum occurs in the mutual information function.⁷ The time delay corresponding to the first minimum in the mutual information function is the minimum time interval necessary for two variables to become essentially uncorrelated. An attractor reconstructed by using τ as the delay time will have uncorrelated components while avoiding the "folding" typical of using values of time delay that are too large.

The mutual information function is similar to the autocorrelation function except that it measures the general dependence of two variables rather than only the variable's linear dependence. Note that random data will be uncorrelated, thus, the mutual information function can be used to indicate if a time series contains correlated information from a deterministic source or if the time series is simply random noise.

The derivation of the mutual information function for two series of measurements S and Q , $I(S,Q)$, is given in [7]. The resulting expression for $I(S,Q)$ is

$$I(S, Q) = H(S) + H(Q) - H(S, Q) , \quad (2)$$

where H is the entropy of the series of measurements.

If the series of N measurements S is given by $(s_1, s_2, s_3, \dots, s_N)$, then the entropy, $H(S)$, is given by

$$H(S) = - \sum_{i=1}^N P_s(s_i) \log_2 [P_s(s_i)] , \quad (3)$$

where $P_s(s_i)$ is the probability of a measurement being equal to s_i .

In a similar manner, if $S = (s_1, s_2, s_3, \dots, s_N)$ and $Q = (q_1, q_2, q_3, \dots, q_N)$ are two sets of measurements, then the entropy of the combined set of measurements, $H(S, Q)$, is given by

$$H(S, Q) = - \sum_{i=1}^N \sum_{j=1}^N P_{sq}(s_i, q_j) \log_2 [P_{sq}(s_i, q_j)] , \quad (4)$$

where $P_{sq}(s_i, q_j)$ is the probability of q_j occurring if s_i is known to occur. In this application, S corresponds to the time series and Q is obtained from S by delaying S by ΔT .

The mutual information is calculated by using equations (2), (3) and (4) for a range of delay times. For a deterministic time series, plotting the values of $I(S, Q(\Delta T))$ (where the dependence of Q on the delay time is explicitly shown) against delay time results in an initially decreasing values of $I(S, Q(\Delta T))$ as delay time increases. $I(S, Q(\Delta T))$ eventually will pass through a minimum and will then vary, always remaining at a relatively low value. The value of delay time at which the first minimum of $I(S, Q(\Delta T))$ occurs is the reconstruction delay time, τ , selected to perform the attractor reconstruction.

2.1.3 - Method of global false nearest neighbors

The method of global false nearest neighbors is based on a simple geometric concept: if the number of dimensions d used to reconstruct an attractor is too small, many points that appear “near” will become widely separated when $d + 1$ dimensions are used in the attractor reconstruction.⁸ Nearest neighbor points that experience this wide separation when comparing their distances in dimension d and $d + 1$ are false nearest neighbors in dimension d . Conversely, true nearest neighbors will remain near each other in attractor reconstructions of both d and $d + 1$ dimensions. The adequacy of dimension d for reconstructing an attractor can be evaluated by selecting a number of random points and their nearest neighbors in dimension d and then calculating the percentage of false nearest neighbors.

Typical results of this calculation for noise free data show the percentage of false nearest neighbors to be relatively high for low dimensional attractor reconstructions, with the percentage of false nearest neighbors decreasing with increasing dimension, eventually reaching and remaining at a value near zero. The lowest dimension corresponding to this minimum value of the percentage of false nearest neighbors is the embedding dimension, d_e . Noisy data show similar

results, except the percentage of false nearest neighbors reaches a minimum at d_e and then increases with increasing dimension. The minimum percentage of false nearest neighbors will not approach zero for noisy data; the amount of random noise contamination will determine the value of the minimum in the global false nearest neighbors calculation results.

A pair of points are considered false nearest neighbors in dimension d if

$$\frac{R_{d+1}^2(n)}{R_d^2(n)} > R_{tol} , \quad (5)$$

where $R_d(n)$ is the Euclidean distance between the n th point and its nearest neighbor in d dimensions, $R_{d+1}(n)$ is the Euclidean distance between the n th point and its nearest neighbor in $d + 1$ dimensions, and R_{tol} is the first criteria for declaring nearest neighbor pairs to be false.⁸ A second criteria, needed because near neighbors may not be especially “close”, is given by

$$\frac{R_{d+1}^2}{\sigma^2} > A_{tol} , \quad (6)$$

where σ is the standard deviation of the time series and A_{tol} is the second criteria for declaring nearest neighbor pairs to be false.⁸ A nearest neighbor pair are declared false if either test (equations (5) and (6)) fails. In our work, the values used for the criteria in equations (5) and (6) have been $R_{tol} = 17.1$ and $A_{tol} = 1.8$.

2.1.4 - Description of radial basis function maps

Previous work has shown that good one-step prediction accuracy can be obtained by using radial basis function maps.⁹ The general form of maps composed of radial basis functions is given by

$$x_{i+1} = \sum_{n=1}^N \lambda_n \phi_{n,i}(\|x_i - \alpha_n\|) , \quad (7)$$

where x is the time series variable, I is the i th iterate, N is the number of terms in the map, λ_n is the coefficient (or weight) of the n th term, $\phi()$ is the radial basis function, and α_n is the n th basis vector or center.¹⁰ Note that the Euclidean norm between the point x_i and the center α_n is the argument supplied to the function $\phi()$. Following the example described in [10], the form of the radial basis function $\phi()$ used in this work is given by

$$r = (\sum_{k=1}^{d_e} (x_{i,k} - \alpha_{n,k})^2)^{\beta},$$

here $\beta > 0$, $\beta \neq 0$, and C is a constant. Substituting the Euclidean norm into equation 8 for r yields the form for the radial basis function proposed for this work:

$$\phi_{n,i} = \left(\sum_{k=1}^{d_e} (x_{i,k} - \alpha_{n,k})^2 + C^2 \right)^{-\beta}. \quad (9)$$

λ_n N data points. This fitting results in the

$$\{x\}_{i+1} = \{\Phi\} \{\lambda\}, \quad (10)$$

where $\Phi = \phi$. Singular value decomposition has been used to determine the values of the λ that give the best prediction of the x_{i+1} .

Two examples of map performance are given in this section. The first example is from a map from the noise created by air blowing over a microphone.

3.1 - Example 1 - The Lorenz System

system has been a ‘workhorse’ for nonlinear dynamic studies because it exhibits rich nonlinear behavior. The Lorenz system is given by

$$\frac{dX}{dt} = Y - X \quad (11)$$

$$\frac{dY}{dt} = r - Y - XZ \quad (12)$$

and

$$\frac{dZ}{dt} = bZ - XY \quad (13)$$

where σ , r , and b are constants and X , Y , and Z are the time dependent coordinates.¹¹

Equations (11), (12), and (13) were integrated by using a fourth-order Runge Kutta numerical integration algorithm. Values of $\sigma = 10$, $r = 28$, and $b = 8/3$; initial conditions of $X = 0.01$, $Y = 0.02$, and $Z = 0.15$; and an integration step size of 0.0005 seconds were used in the calculation. Values of X , Y , and Z were tabulated for 0.005 second intervals.

The attractor used in the map calculation was obtained from the X coordinate by using the method of delays. The optimum time delay for the reconstruction was set equal to the first minimum in the mutual information function and corresponded to 30 samples. The embedding dimension was calculated to be 4 based on the minimum value of the global false nearest neighbor calculation. A 90-term radial basis function map was used to model the time series. K-means clustering was used to select the 90 centers from the attractor; it is felt that selecting the centers in this way ensures that the centers are reasonably representative of the entire attractor.

A comparison of the calculated and the map-predicted values of the time series is shown in figure 1. Note that the calculated and the predicted values are nearly identical. The ability of the map to predict the time series so accurately is due mainly to the fact that the time series is noise free. Map error becomes larger for noisy real-world time series.

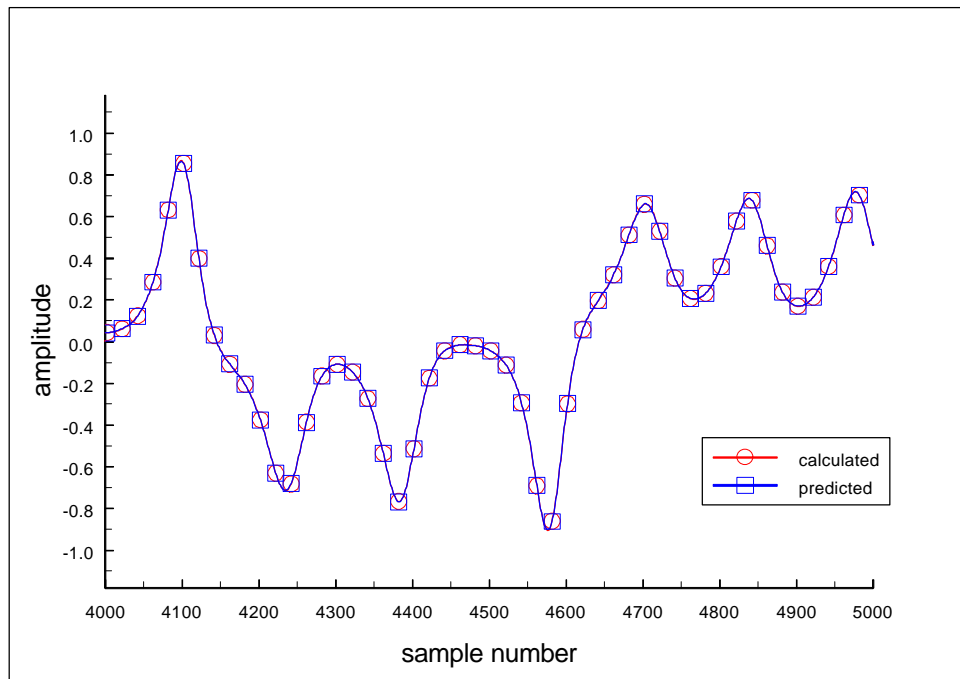


Figure 1. Comparison of calculated and map-predicted values for the Lorenz system. The values have been normalized to be between +1 and - 1.

3.2 - Example 2 - A Recorded Time Series

The second example uses a recording made of air from a fan blowing over a microphone as the time series. The recording was digitized at a sample rate of 11025 Hz and stored as 16-bit integers. The frequency response of the microphone is unknown but is not believed to be of particularly high fidelity. The time series is shown in figure 2.

The optimum time delay for the reconstruction was again set equal to the first minimum in the mutual information function and corresponded to 38 samples. The embedding dimension was calculated to be 4. A 90-term radial basis function map was used to model the time series.

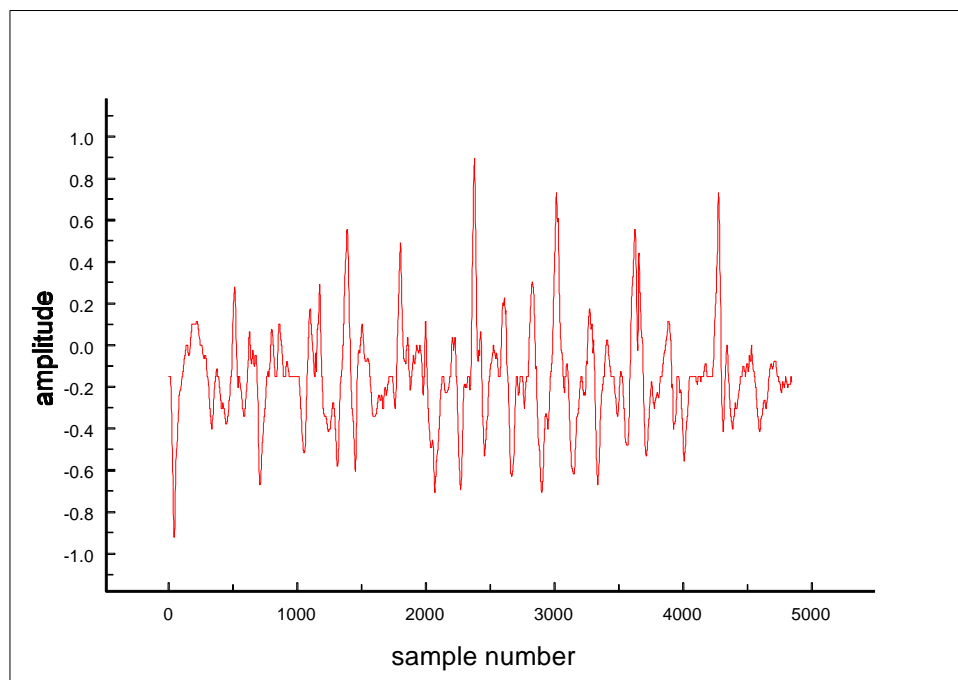


Figure 2. The normalized time series obtained from the recording.

A comparison of the calculated and the map-predicted values of the time series is shown in figure 3. The map accurately predicts the recorded time series but that the agreement between the measured and predicted values is poorer than was obtained with the Lorenz system. The poorer agreement is attributed to the presence of random noise in the recorded signal.

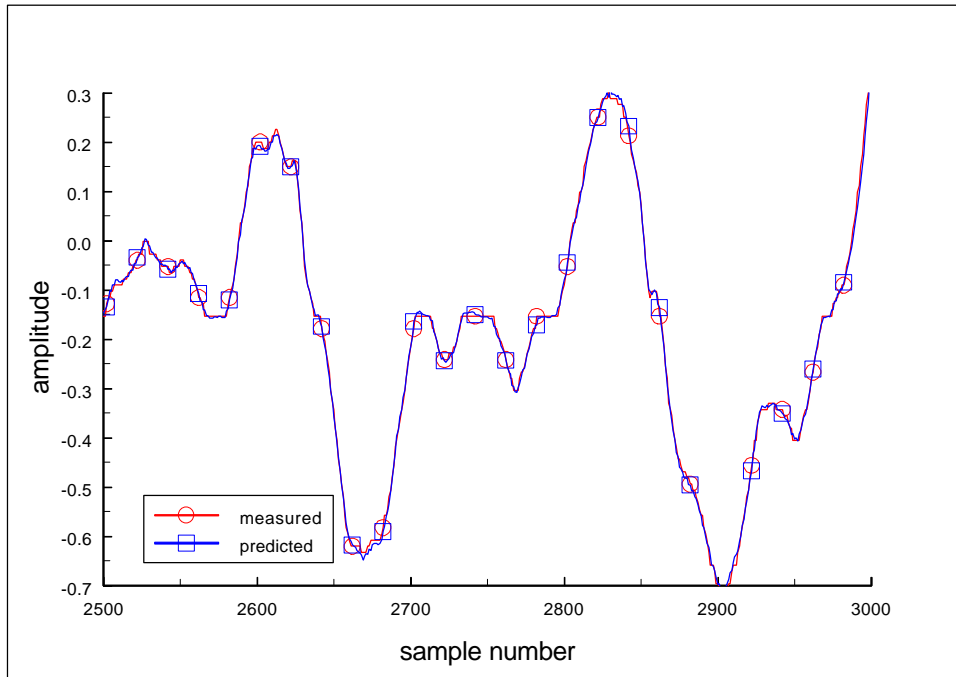


Figure 3. Comparison of the measured and predicted time series for the recorded data.

4. - APPLYING ONE-STEP PREDICTION MAPS TO THE PROBLEM OF MACHINE OR PROCESS SYSTEM DIAGNOSTICS

The application of one-step prediction maps for diagnosing machinery or process system condition is straight forward. A baseline time series is collected from the machine or system during normal operation. The nonlinear time series analysis techniques described above are applied and a suitable one-step prediction map is created. This map is then used to calculate the average map error for the baseline time series.

Once the one-step prediction map and the average absolute map error for the baseline time series are obtained, monitoring is performed by using the one-step prediction map to periodically calculate the average absolute map error using a current time series. The current value of map error is compared with the map error for the baseline time series. A significant increase in the map error indicates that a change in the system has occurred.

It seems unlikely that the determination of what constitutes a “significant” map error change can be made without resorting to data collected from the machine or system operating over a range of conditions. Thus, before one-step prediction maps can be used for monitoring, map errors for a range of known conditions should be calculated. These map errors can then be used to determine whether a given map error change is significant or falls within normal variations.

A variation of this approach is to calculate one-step prediction maps for each of the known conditions. A crude diagnosis could be performed by calculating the map error for a given time series using one-step prediction maps corresponding to each known condition. The current condition would be diagnosed as being the one corresponding to the condition used to create the one-step prediction map that gives the smallest map error.

5. - APPLICATION RESULTS

Use of one-step prediction maps as indicators of changes in dynamic systems was investigated by using simulated and measured time series. Advantages of using simulated time series in the evaluation are that dynamic system changes are of known magnitude, occur at known times, and the time series are noise free. The advantage of using a measured time series in the method evaluation is that the method performance can be evaluated under real-world conditions, where noise and uncertainty exist. The use of both simulated and measured time series provides a reasonable evaluation of the method's potential for use in machine or process system diagnostics.

5.1 - Test of the Diagnostic Method by Using a Simulated Time Series

The first tests of the diagnostic method were performed by using a simulated time series. The Lorenz system of equations was selected as the dynamic system. This system experiences chaotic behavior for a proper choice of the parameters σ , r , and b . In this work $\sigma = 10$ or 12 , $r = 28$, and $b = 8/3$; these values result in chaotic dynamic behavior.

5.1.1 - Effect of parameter change on the average map error

Three time series spanning a period equivalent to 400 seconds were created by integrating equations 11, 12, and 13. The calculated data was recorded for time intervals of 0.005 seconds. A σ value of 10 was used during the first 200 seconds and a σ value of 12 was used during the final 200 seconds. The initial 100 seconds of data were discarded to avoid the initial transient.

The time series corresponding to the X component was used in the test. The calculated first minimum in the average mutual information function was equal to 0.16 seconds and the calculated embedding dimension was 5. A 90-term radial basis function map was created by fitting the first 10000 stored time series points; these points were calculated by using a value of $\sigma = 10$. The map error was calculated for each point in the time series and evaluated for an indication of the change in the value of σ at $t = 100$ seconds.

Figure 4 shows the map error for entire time series. During the first 100 seconds, the average map error equals -0.0008 and the standard deviation = 0.00186. During the final 200 seconds, the average map error equals -0.00018 and the standard deviation = 0.00338. The average map error clearly indicates that a parameter change, i.e., a change in the system dynamics, occurred at approximately $t = 100$ seconds. These results show that for a noise-free time series, the average map error can indicate a change in system dynamics. Furthermore, if a dynamic change occurs at a

particular time τ , the effect of that dynamic change on the map error will occur at the time $\tau + \Delta\tau$, i.e., one sample after the change occurs.

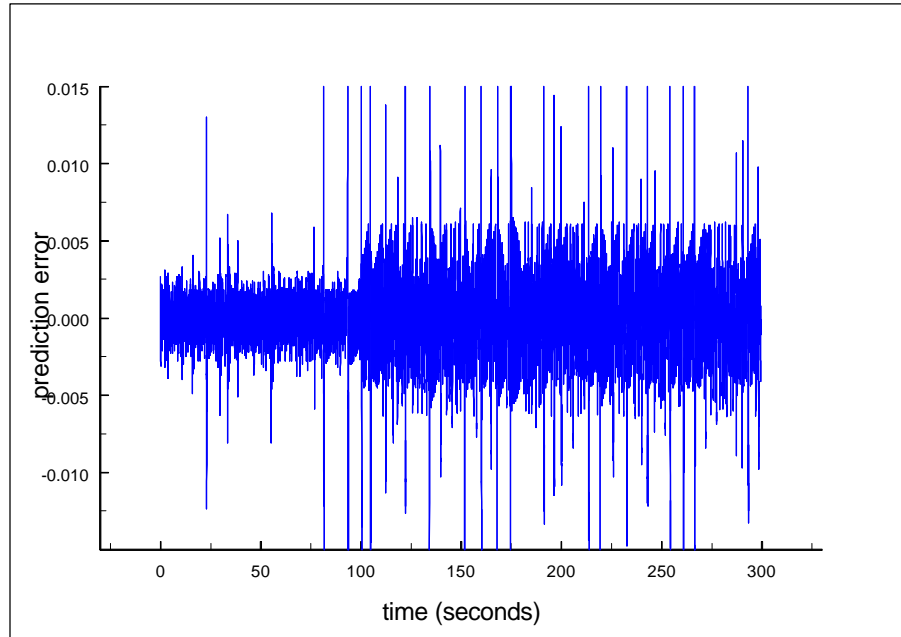


Figure 4. The prediction error for the Lorenz time series. Note the discontinuity at $t = 100$ seconds.

5.1.2 - Effect of adding a sine wave to the time series

A second example using simulated data involved adding a sine wave of unit amplitude and a frequency of 1 Hz to the X component for $t > 100$ seconds. The previously-calculated 90-term radial basis function map was used in this example. The map error was calculated for the time series and transformed into the frequency domain.

Figure 5 compares the frequency spectrum for the map error time series containing the added sine wave ($t > 100$ seconds) with the frequency spectrum for the map error time series with no sine wave ($t < 100$ seconds). Note that the 1 Hz component is clearly visible in the spectrum containing the sine wave and that the amplitude of this spectrum is considerably greater than that of the spectrum without the sine wave, a finding consistent with the results of the previous example.

Figure 6 compares the frequency spectra of the X component of the Lorenz attractor with the added sine wave with the X component of the Lorenz attractor with no sine wave. The comparison shows no significant differences between the two spectra. These results indicate that the map error

may be a sensitive indicator of changes in the time series dynamics and that its frequency domain may be superior to its time domain for detecting changes in a time series.

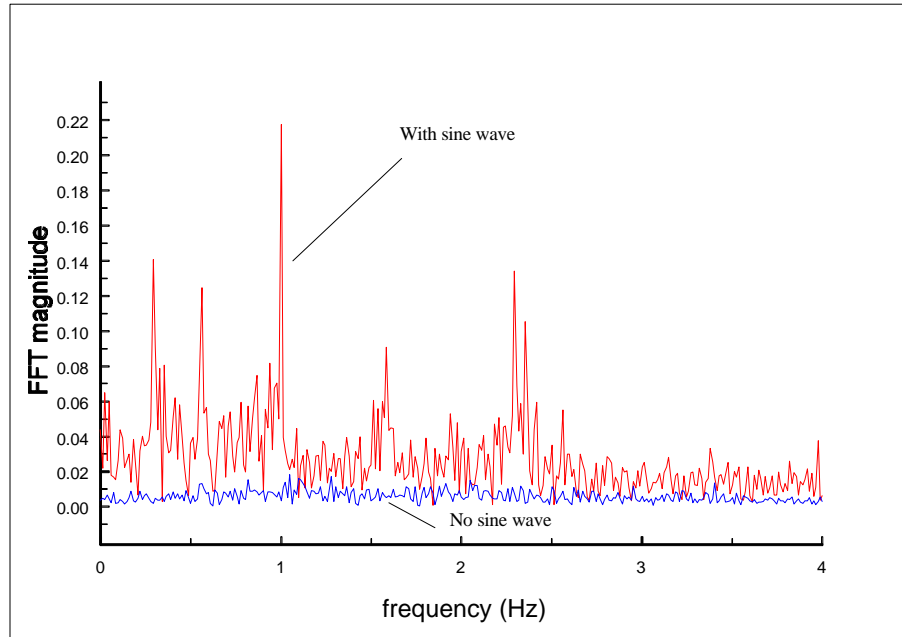


Figure 5. Comparison of the map error spectra with and without the added sine wave.

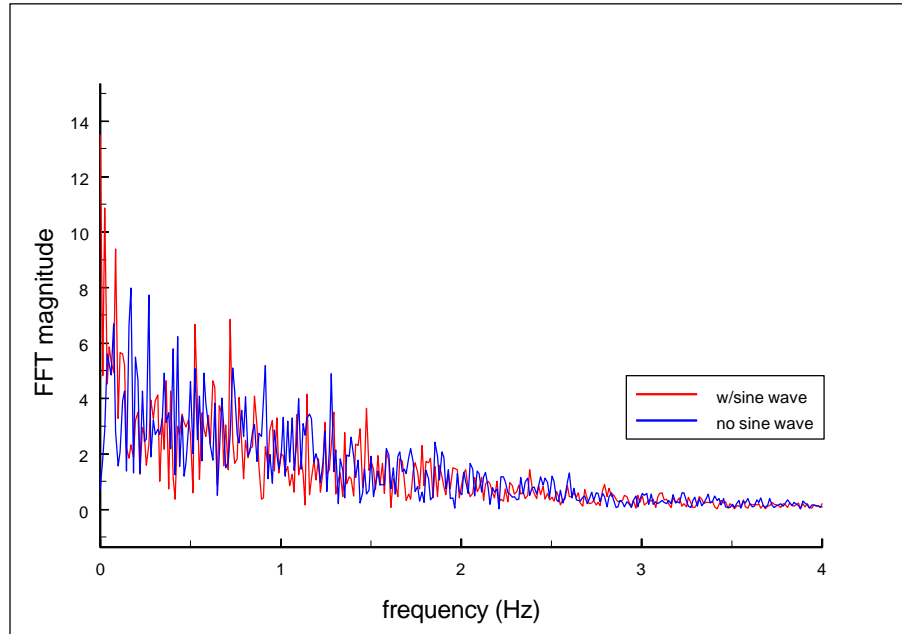


Figure 6. Comparison of the spectra of the Lorenz attractor X component with and without the added sine wave.

Comparing figures 5 and 6 show that the sine wave is not detectable in the time series spectra, but is easily detected in the map error spectra. This result implies that a dynamic change may be detectable in the map error spectrum before it could be detected in a spectrum formed from the measured time series. More generally, the results of investigating the effects of adding a sine wave to a time series agree with the previously shown results; the map error is seen to be very sensitive to changes in time series dynamics. In addition, the results show that if a dynamic change occurs at a particular frequency, the effect of the dynamic change on the map error will occur at that same frequency. This result is important because many common machinery faults occur at known ratios of the machine operating speed. Thus, the same diagnostic rules used to interpret machinery vibration spectra may be applied to interpret map error spectra.

5.2 - Test of the Diagnostic Method by Using a Measured Time Series

The diagnostic method was tested by using radio frequency (RF) data collected at an industrial plant for the purpose of detecting electrical arcing in motors. Two data sets were used. The first data set was inadvertently low-pass filtered, resulting in a data set that contained no information indicative of arcing (arcing is a high-frequency phenomenon). The second data set was high-pass filtered and was useful for detecting arcing. For both data sets, the data was collected for two seconds at a sample rate of 2 MHZ and low-pass filtered using a cut-off frequency of 1 MHZ to avoid aliasing. The low-frequency data was used to investigate the effectiveness of the average absolute map error for detecting changes in motor current. The high-frequency data was used to investigate the effectiveness of analyzing the map error time series for detecting arcing.

5.2.1 - Average absolute map error

The first data set was inadvertently low-pass filtered using a cut-off frequency of 10 KHZ (this second filtering wasn't discovered until after the analysis was completed). Separate data files were collected for different values of motor current. A summary of the data files is shown in Table 1.

Table 1 - Summary of RF Data Files

File Designator	Motor Current (amperes)
1,2, & 3	26
4, 5, & 6	61
7, 8, & 9	123
10, 11, & 12	160
13, 14, & 15	202
16, 17, & 18	221
19, 20, & 21	249

A time series taken from data file 1, which corresponds to the lowest motor current value used in the test, was used as the baseline time series. This data was low-pass filtered, down sampled by a factor of 30, and used to form a 30,000-point baseline time series. The down sampling was performed to allow a larger time interval to be used in the map error calculation without making the number of points in the baseline time series unwieldy. A 90-term radial basis function map was created by using a reconstruction time delay of 54 samples and an embedding dimension of 8.

High correlation between the average absolute map error and the motor current is shown in Figure 7. This result indicates that map error is sensitive to changes in real systems (in this case motor current) and may be sufficiently robust to be used with measurements. The map error fails to show arcing because of the data being low-pass filtered at 10 KHZ.

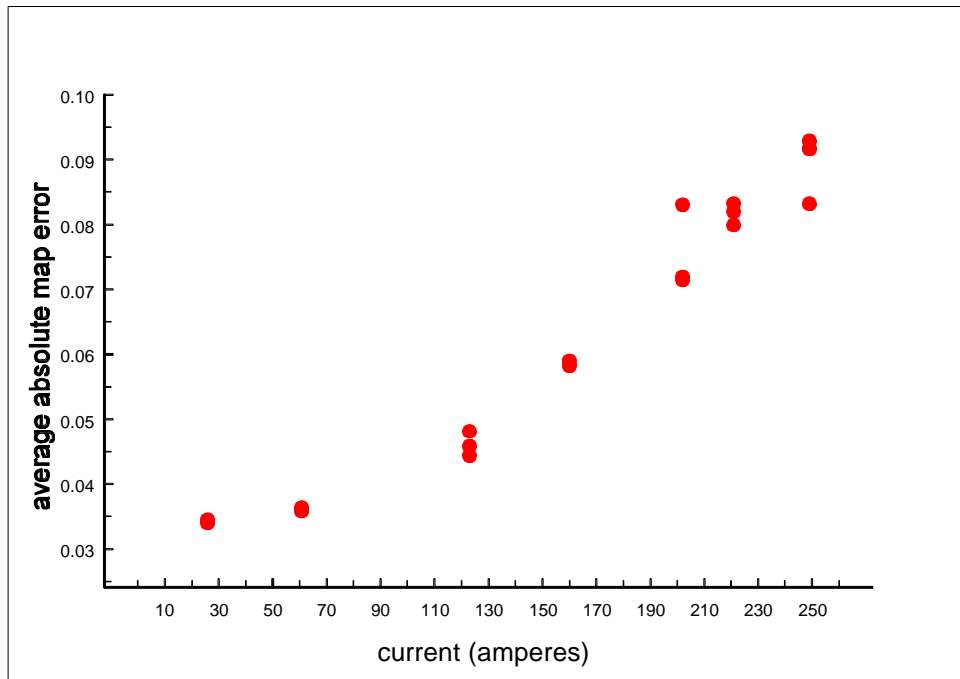


Figure 7. Average absolute map error for different motor current values.

5.2.2 - Analysis of the Map Error Time Series

The second attempt at using map error to detect arcing involved analyzing the time series of the map. RF data was collected for motor currents of between 25 and 300 amperes and with the motor brushes in the ~4 bar position. Four-million point data files were stored for each combination of motor current and brush position. Table 2 gives the conditions corresponding to the data files used in the evaluation.

Table 2. Summary of High-Frequency Data Files

Condition	File Name	Motor Current (amperes)	Brush Position
no arcing	A3.055.txt	28	~4.0 bar
no arcing	A3.057.txt	58	~4.0 bar
no arcing	A3.059.txt	120	~4.0 bar
light pin fire	A3.061.txt	198	~4.0 bar
medium arcing	A3.063.txt	249	~4.0 bar
heavy arcing	A3.066.txt	300	~4.0 bar

Figure 8 shows the Fast Fourier Transform (FFT) magnitude of the RF data collected during non-arcing conditions. Figure 9 shows the FFT magnitude of the RF data collected during heavy arcing. Comparing the two frequency spectra reveals little qualitative difference between the two spectra and shows why attempting to detect arcing from the RF data is so difficult. Note that the time series used to calculate these FFT's were normalized to be between ± 1 for use in map creation. The one-step prediction map used in the map error evaluation was formed by using thirty thousand data points from a baseline time series collected for non-arcing. Nonlinear analysis showed that the baseline time series had an embedding dimension of six and an attractor reconstruction time delay of 9.0×10^{-6} seconds (this time delay corresponds to 18 samples). These nonlinear parameters were used to form a 50-term radial basis function map. The baseline map error time series is shown in Figure 10.

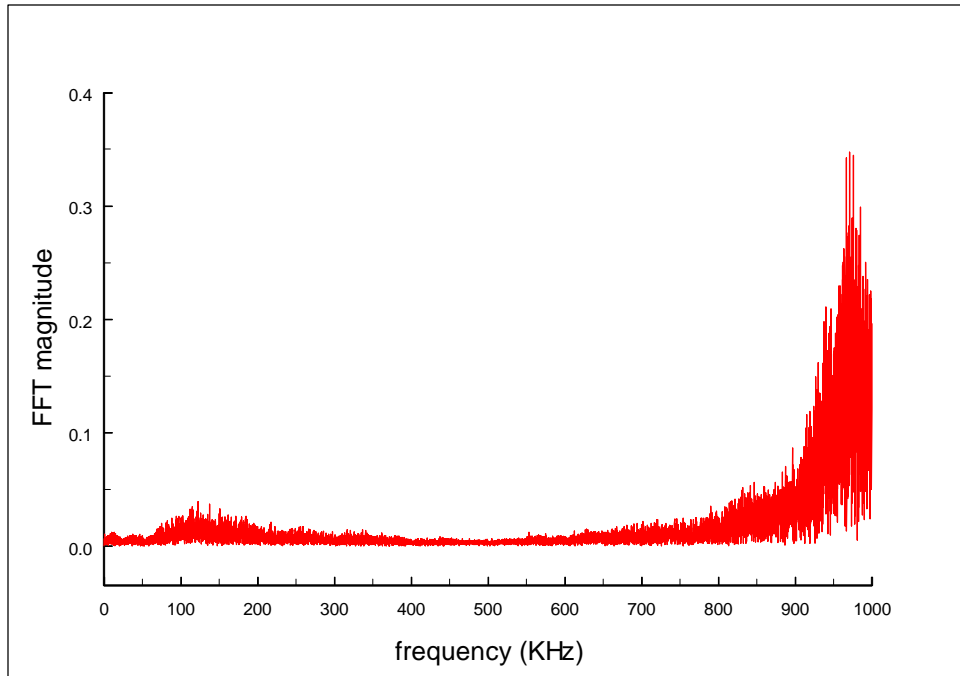


Figure 8. FFT magnitude of normalized RF data collected during non-arcing conditions.

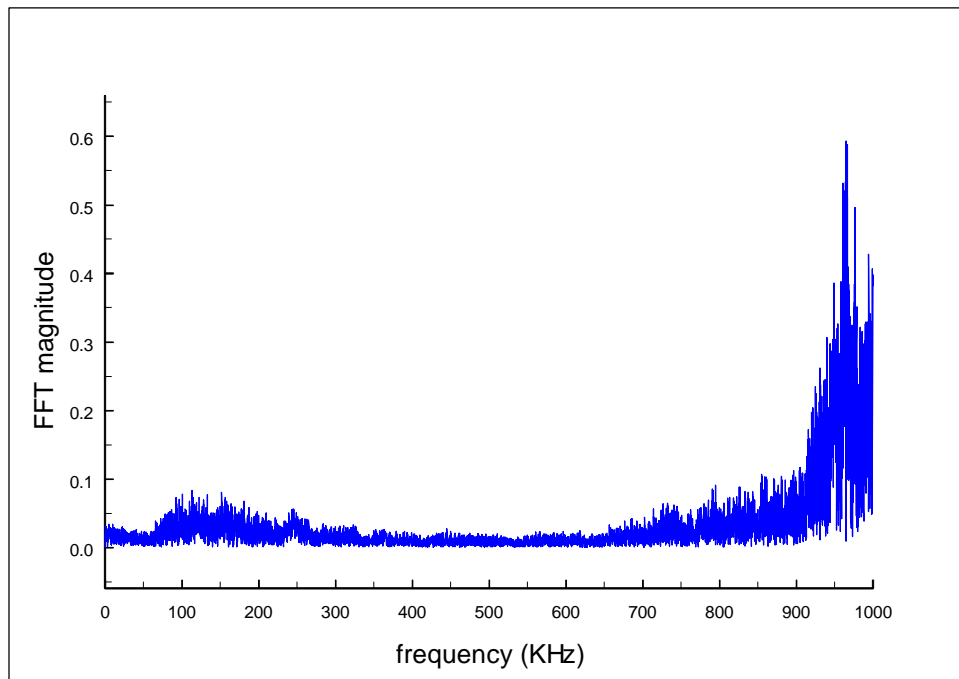


Figure 9. FFT magnitude for normalized RF data collected during heavy arcing.

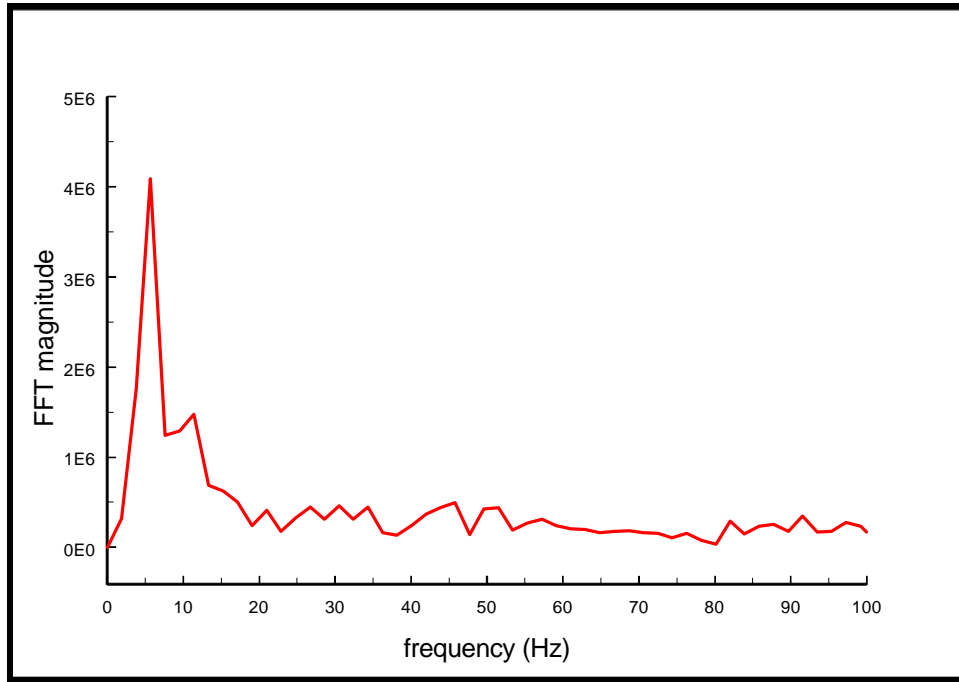


Figure 10. Variation of map error power in the frequency domain.

5.2.2.1 - Analysis of map error power

One useful descriptor characterizing the map error time series is the total power, P_t , given by

$$P_t = \sum_{i=1}^N Me_i^2, \quad (14)$$

where Me is the map error time series and N is the number of time series points. Time-dependent behavior of the total map error power was calculated by taking a series of 32768-point Fast Fourier Transforms (FFT's) with each data block overlapping all but 512 points of the previous data block. Figure 11 shows the time-dependent behavior of the map error power for the baseline time series; the FFT magnitude of this time series is shown in figure 12. These results show that the map error power (and the map error itself) oscillates at the motor rotational frequency of five Hz. Closer inspection of Figure 10, which corresponds to one full revolution of the motor, shows a small amplitude region during the first half of the revolution (for times less than 0.1 second) and a larger amplitude region during the second half of the revolution (between 0.1 and 0.2 seconds). This behavior is responsible for the oscillations shown in figures 11 and 12.

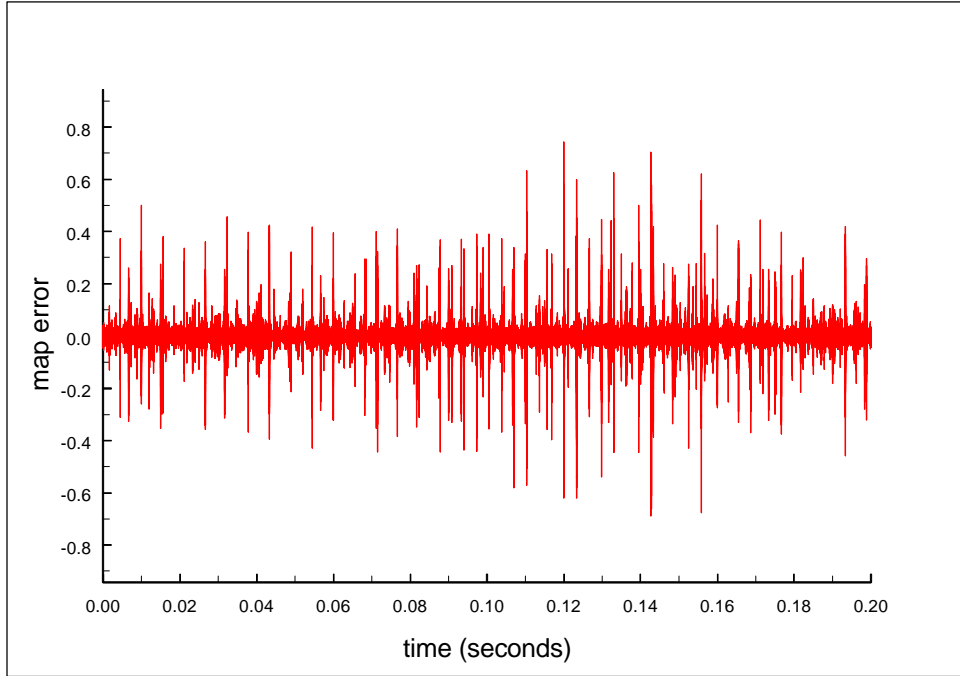


Figure 11. The map error time series for the baseline time series (file A3.055.txt).

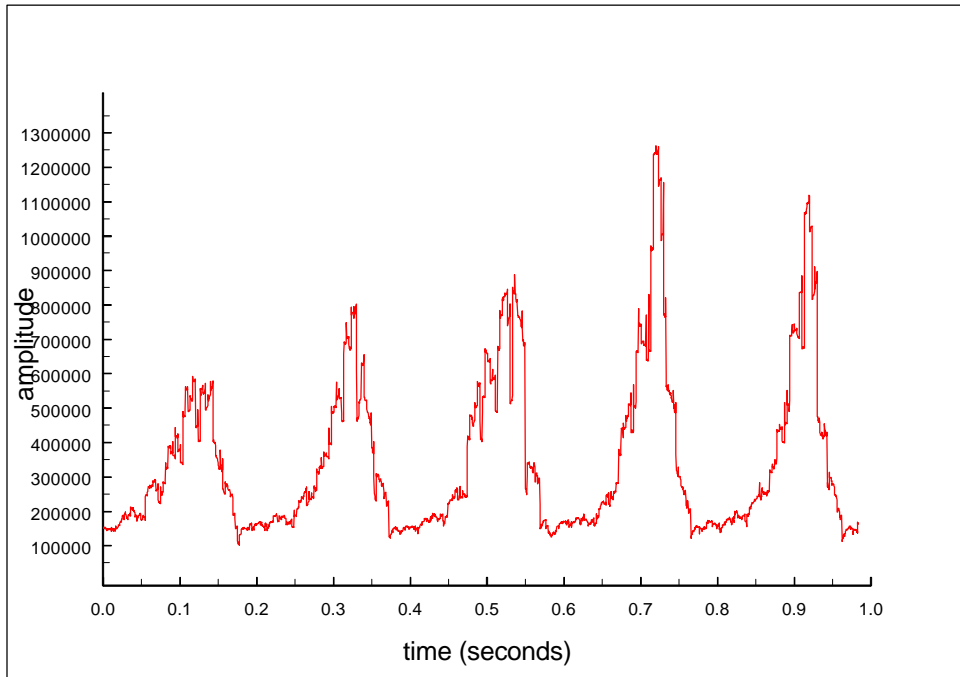


Figure 12. Variation of map error power in the time domain. The map error was calculated by using a map formed from the first 50000 points in the baseline time series.

There was some initial concern over the source of the five Hz oscillation; it was speculated that the oscillation could be an artifact of the map coefficient calculation. Because the map is calculated by using data points corresponding to a small fraction of a single revolution, it may be possible for the map to not accurately represent the dynamics of the entire revolution. If this were the case, a map error that oscillates at the running speed would be expected.

To investigate this possibility, a second one-step prediction map was created by using data points corresponding to the high amplitude portion of figure 12. Comparison of the map error power time series would then show if the oscillation was caused by the map coefficient calculation or is a true feature of the data. If the high-amplitude part of the map error time series is caused by a variation in the system dynamics over one motor revolution, then a relatively small amplitude should occur for that part of the motor revolution used in the calculation of the map coefficients. If the high-amplitude part of the map error time series is a true signal feature, then the two map error power time series will be qualitatively the same.

A one-step prediction map was formed from 30,000 data points from the baseline time series beginning 0.1 seconds from the start of the time series (i.e., during the high amplitude portion of the time series shown in Figs. 10). The map error time series formed by applying this map to the baseline time series is shown in Figure 13. The results are qualitatively the same as those shown in Figure 11. Because the low and high amplitude sections appear over the same portion of motor revolution, it can be concluded that the five Hz oscillation is a feature of the signal and is not an artifact of how the map coefficients were calculated.

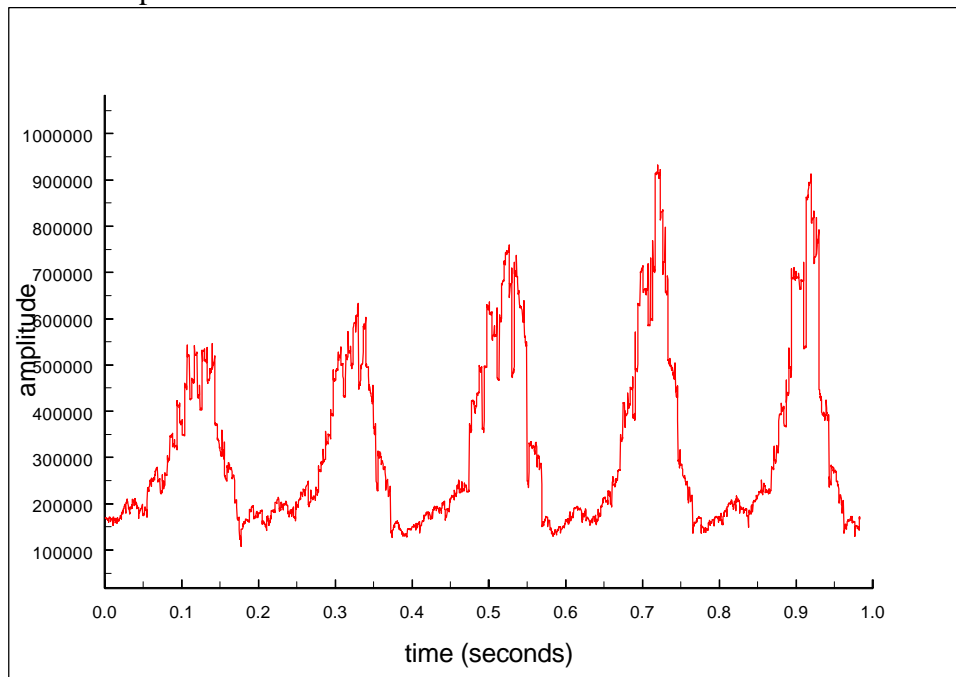


Figure 13. Variation of map error power in the time domain. The map error was calculated by using a map formed by using 50000 points beginning at $t = 0.1$ seconds in the baseline time series.

5.2.2.2 - Power ratio - an arcing discriminator

The power ratio used as an arcing discriminator is calculated by dividing the power in the map error time series between 900 KHZ and 1 MHZ by the total power. This ratio was suggested after comparing map error time series in the frequency domain for non-arcing and arcing conditions. Figure 14 shows the FFT magnitude of the baseline map error time series (non-arcing). The FFT magnitude has a large amplitude region between 100 KHZ and 200 KHZ with small amplitudes at higher frequencies. Figure 15 shows the FFT magnitude of the map error time series for RF data collected during heavy arcing. This FFT magnitude has a large amplitude region above 900 KHZ. The ratio of the power for frequencies greater than 900 KHZ to the total power should have a small magnitude for non-arcing and a large magnitude when arcing occurs.

The power ratio was calculated for each of the available data files. The data was divided into 8192-point data blocks with each data block overlapping all but 512 points of the previous data block. Each block was transformed into the frequency domain and the power ratio was calculated. The average power ratio was then calculated for each data file. The calculation results are shown in Figure 16 and tabulated in Table 3.

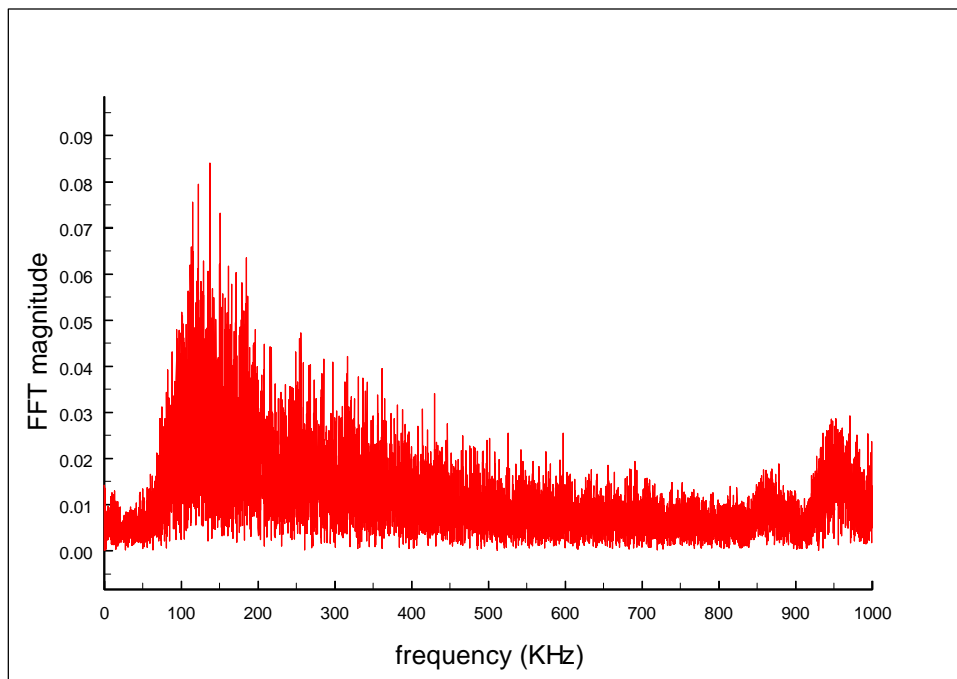


Figure 14. FFT magnitude of a map error time series collected during non-arcing conditions.

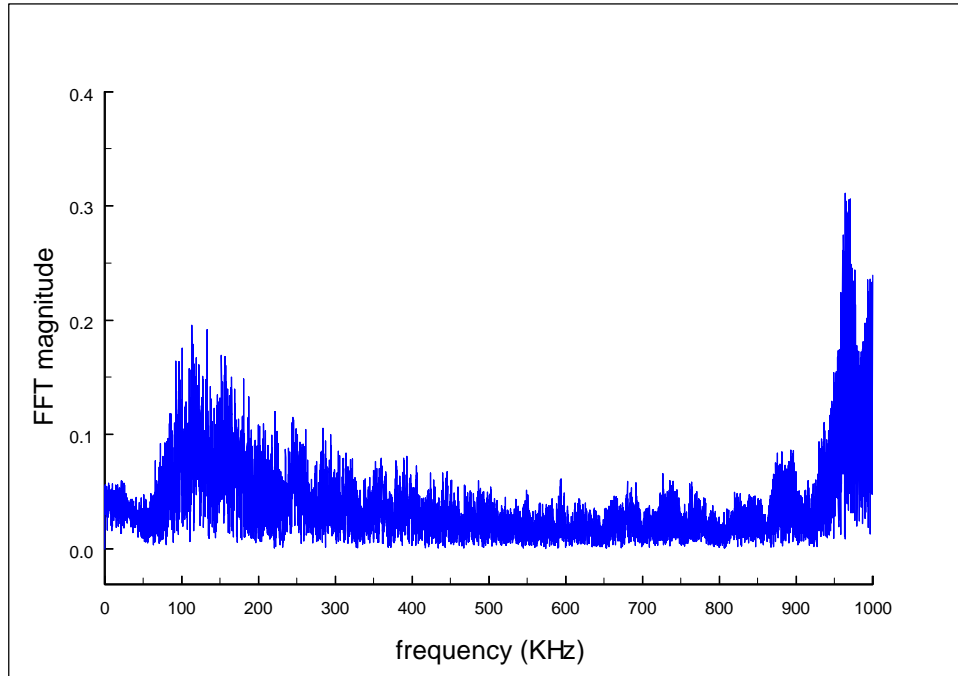


Figure 15. FFT magnitude of a map error time series collected during heavy arcing.

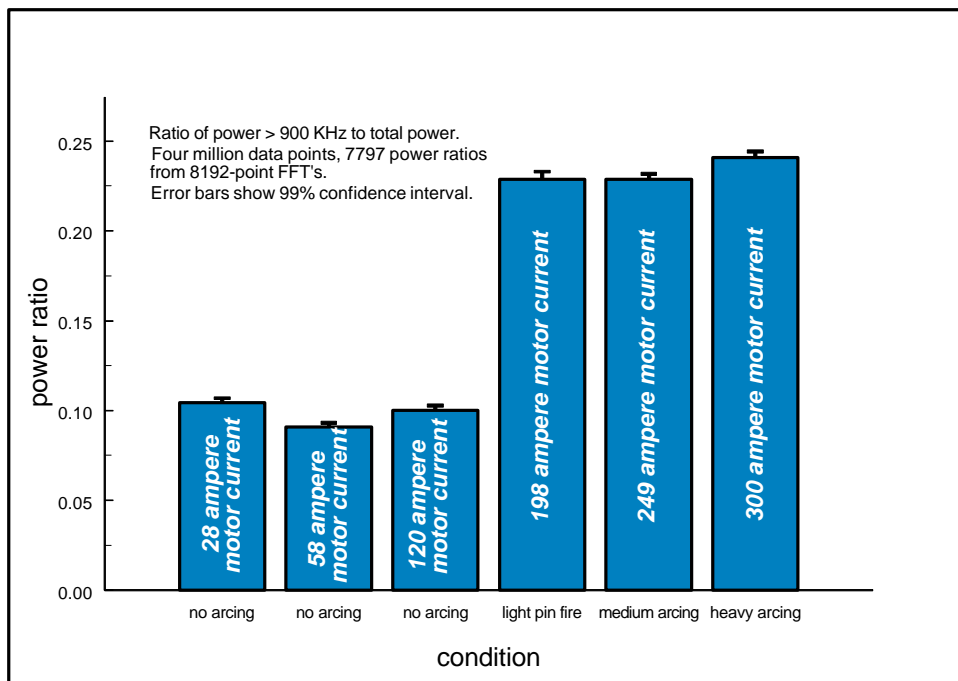


Figure 16. Power ratio for conditions ranging from non-arcing to heavy arcing.

The power ratio appears to be a good discriminator of arcing. The power ratio is approximately twice as large for time series recorded during arcing compared with time series recorded during non-arcing conditions. Furthermore, the results suggest that the power ratio may increase with the severity of the arcing; the power ratio for heavy arcing is greater than those of moderate arcing or light pin fire.

Table 3. Power Ratio for a Range of Arcing Conditions.

Condition	Motor Current (amperes)	Power Ratio	Standard Deviation	99% Confidence Interval
no arcing	28	0.104	0.085	0.0025
no arcing	58	0.091	0.075	0.0022
no arcing	120	0.100	0.085	0.0025
light pin fire	198	0.229	0.142	0.0041
medium arcing	249	0.229	0.111	0.0032
heavy arcing	300	0.241	0.116	0.0034

6. - SUMMARY

The present work indicates that the map error formed by using one-step prediction maps can be used to indicate when a system has experienced a change affecting its dynamics. The ability to detect changes in the time series of dynamic systems such as machinery or process systems allows the map error to form the basis for a form of machine or process system diagnostics. This form of diagnostics can be reduced to an overall measure of “sameness” characterized by the comparison of the average absolute map errors for baseline and subsequent time series.

6.1 - Research Accomplishments

It has been shown that the map error for a synthetic system (the Lorenz system) can successfully be used to indicate when a system parameter change occurs. Furthermore, it has been shown that in addition to giving an indication characterizing the overall behavior of a time series (i.e., the average absolute map error for a time series), the map error itself forms a time series with enhanced sensitivity to system changes. It has been shown that if a significant change occurs in a

dynamic system at a time τ , the effect on map error time series will occur at time $\tau + \Delta\tau$. Necessarily, if a significant change occurs in a dynamic system at a particular frequency, the map error time series will show the change at that same frequency. This result means that known relationships between running speed and particular faults, which are well known, can be used to diagnose the cause of peaks in map error frequency spectra.

This evaluation of map error as an indicator of motor arcing in RF data is very encouraging. The map error spectra show features indicative of arcing that are not present in the spectra of the RF data. These features can be used to obtain a discriminator, the power ratio, that potentially can be used to detect when arcing occurs.

The comparison of RF data for arcing and non-arcing conditions shows no significant differences between the frequency spectra for these two conditions. Thus, detecting when arcing occurs would be difficult based on the RF data. The map error time series shows a significant increase in power in the higher frequencies when arcing occurs. This finding is not surprising, because the map error is a sensitive indicator of change from the baseline condition used during map formation and arcing is known to occur at high frequencies. Thus, the map error contains significant energy at high frequencies when arcing occurs.

A simple discriminator indicative of arcing is the power ratio, which is the power in the map error time series for frequencies greater than 900 KHZ divided by the total power. The numerical value of power ratio is small for non-arcing conditions but increases when arcing occurs because of the increase in high-frequency energy. Results using the high-frequency data show that the power ratio approximately doubles during arcing.

The power ratio is highly variable, a fact shown by its large value of standard deviation. This large value is caused by the 5 Hz oscillation in total power shown in Figs. 10, 11, and 12. The cause of this oscillation is unknown, but is clearly a feature of the signal and is not an artifact of map creation.

6.2 - Areas for Future Research

Map error, either as an overall indicator of time series “sameness” or as a time series analyzed independently, shows promise for performing machine or system diagnostics. The current results indicate that further exploration of the potential of this approach is warranted. Further exploration in the area of diagnostics should concentrate on evaluating the effectiveness of map error for detecting changes in measured time series obtained from either machinery or process systems.

It is likely that map error may be useful for other applications. Speaker and/or word recognition and sensor validation are two applications that have already been partly explored. Medical applications appear to be a natural extension of the current diagnostic work. Innovative uses for map error and map error diagnostics may be a useful approach for a number of additional applications.

6.3 - Efforts to Secure Follow-on Funding

Information gained and results generated from this investigation will be useful in the preparation of proposals and white papers. Several areas appear particularly promising regarding future use of the method. In the area of predictive maintenance, detection of arcing certainly is a problem that can be solved by using this method. It would not be unreasonable for companies, such as Alcoa, with a large number of electric motors, to be targeted as likely sponsors of follow on work. The Navy has a great interest in predictive maintenance for surface ships (i.e., the “Smart Ship Program”), so they may also be a likely source of follow-on funding for this effort. Medical diagnostics may be another promising area for the method’s application. Recently representatives from Biomec, Inc. have shown some interest in the potential of the method for interpreting EKG signatures. National Security Programs Office contacts have an interest in speaker and/or word identification; map error and map error diagnostics may be a useful approach to this problem.

An invention disclosure was submitted for the method and has been elected for filing with the United States Patent office by the LMER Office of Technology Transfer.

REFERENCES

1. J. S. Mitchell, *Machinery Analysis and Monitoring*, Penwell Books, PennWell Publishing Company, Tulsa, Oklahoma, 1981.
2. A. M. Smith, *Reliability-Centered Maintenance*, McGraw-Hill Inc., New York, 1993.
3. J. L. Frarey, "Have We Finished?", *Sound and Vibration*, October, 1995.
4. N. L. Baxter, "In Anticipation of the Forces of Correction, *Sound and Vibration*, June 1996.
5. J. S. Mitchell, "MIMOSA-A Key to Successful Information Age Equipment Asset Management", Proceedings of a Joint Conference: The 51st Meeting of the Society for Machinery Failure Prevention Technology and the 12th Biennial Conference on Reliability, Stress Analysis and Failure Prevention, Virginia Beach, Virginia, April 14-18, 1997, Society for Machinery Failure Prevention Technology, Haymarket, Virginia, 1997.
6. N. H. Packard, J. P. Crutchfield, J. D. Farmer, and R. S. Shaw, "Geometry from a Time Series", *Physical Review Letters*, Volume 45, Pg. 712, 1980.
7. M. Fraser and H. L. Swinney, *Independent Coordinates for Strange Attractors from Mutual Information*, *Physical Review A*, Volume 33, Number 2, pg. 1134 - 1140, February 1986.
8. M. B. Kennel, R. Brown, and H. D. I. Abarbanel, *Determining Embedding Dimension for Phase-Space Reconstruction using a Geometrical Construction*, *Physical Review A*, Volume 45, Number 6, pg. 3403 - 3411, March 1992.
9. B. Damiano and J. E. Breeding, *Application of Polynomial and Radial Basis Function Maps to Signal Masking*, ORNL/TM 13515, Oak Ridge National Laboratory, Oak Ridge, Tennessee, January 1998.
10. M. Casdagli, *Nonlinear Prediction of Chaotic Time Series*, *Physica D*, Volume 35, pg. 335 - 356, 1989.
11. H. G. Schuster, *Deterministic Chaos: an Introduction*, Weinheim, Federal Republic of Germany, 1988.

APPENDIX A
PUBLICATIONS, PAPERS, INVENTIONS, AND PROPOSALS

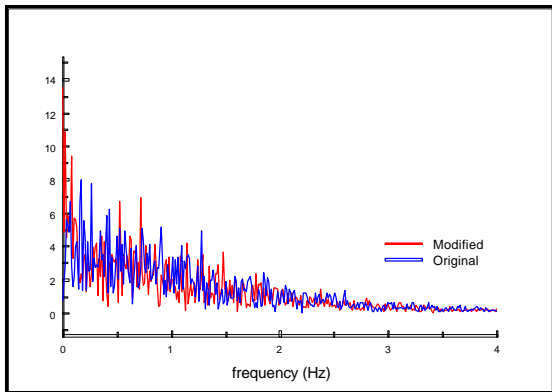
Papers Presented at Technical Meetings

Machine and Process System Diagnostics using One-Step Prediction Maps, B. Damiano, J. E. Breeding, and R. W. Tucker, Jr., MARCON99 Conference, Gatlinburg, Tennessee, May 10-12, 1999. The paper may be found in the MARCON99 Proceedings, Volume 1, pg 9.02.

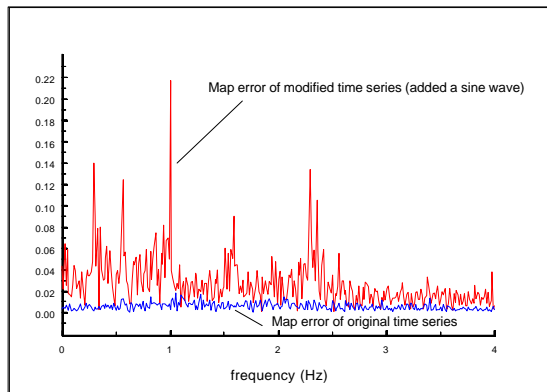
Invention Disclosures

“ERID 0707, S-92,561, “Method to Enhance Features Indicative of Monitored System Degradation.” LMER has elected to file a patent application for this invention, but the patent application had not been filed as of 11/5/99.

Map Error Can be used to Detect Subtle Variations in a Time Series that are Difficult to Detect with other Methods.



FFT of original and modified time series.



FFT of original and modified map error time series.